Electrochemical characterization of Ti3C2T MXene prepared via a molten salt etching route in an acetonitrile-based electrolyte

Liyuan Liu, Encarnacion Raymundo-Piñero, Pierre-Louis Taberna, Patrice Simon

Electrochemistry Communications 148 (2023) 107453

Contents lists available at ScienceDirect

Electrochemistry Communications

journal homepage: www.elsevier.com/locate/elecom

Full Communication

Electrochemical characterization of $Ti_3C_2T_x$ MXene prepared via a molten salt etching route in an acetonitrile-based electrolyte

Liyuan Liu [a,b], Encarnacion Raymundo-Piñero [b,c], Pierre-Louis Taberna [a,b,*], Patrice Simon [a,b,*]

[a] CIRIMAT, UMR CNRS 5085, Université Paul Sabatier Toulouse III, 118, route de Narbonne, 31062 Toulouse, France
[b] RS2E, Réseau Français sur le Stockage Electrochimique de l'Energie, FR CNRS, 3459, 80039 Amiens Cedex, France
[c] CNRS, CEMHTI UPR3079, Université Orléans, Orléans, France

ARTICLE INFO

Keywords:
$Ti_3C_2T_x$ MXene
Molten salts approach
Acetonitrile
Surface termination
Li-ion battery

ABSTRACT

Two-dimensional metal carbide and nitride materials (MXenes) with controlled Cl- and O-surface terminations (MS-$Ti_3C_2T_x$) were prepared by a molten salt etching route and their electrochemical properties were investigated in nitrile-based electrolytes. The results show that the power performance of MS-$Ti_3C_2T_x$ was greatly improved in acetonitrile (ACN)-based non-aqueous organic electrolytes, which are conventional electrolytes for electrochemical capacitors. The addition of a lithium salt to produce 2 M LiTFSI in ACN results in an increase in the specific capacitance. Moreover, replacing LiTFSI by LiFSI drastically improves the power performance of MXenes at a high scan rate (95 mAh g^{-1} at 900C). These results highlight the importance of properly matching the electrolyte composition to the electrode material and shed light on MXenes as high-rate electrode materials for energy storage applications.

1. Introduction

MXenes are a diverse class of layered two-dimensional (2D) transition metal carbides or carbonitrides with the general formula $M_{n+1}X_nT_x$ (n = 1–3), where M represents an early transition metal, X is carbon and/or nitrogen and T_x represents surface groups originating from the etchant [1–4]. Since their discovery in 2011, MXenes have been regarded as very promising 2D materials in various fields, especially in the world of electrochemical energy-storage applications, thanks to properties including metal-like electrical conductivity, controllable layer spacing, tunable surface chemistry, and rich chemical composition [1–7]. Over the past 10 years, MXenes have generally been prepared by the etching of MAX phases (where A is an A-group element) in aqueous solutions containing fluoride ions (HF [6], LiF + HCl [2]), which give rise to -F and –OH-containing surface-functionalized MXenes (HF-MXenes). Many research studies have revealed that tuning the surface functional groups of MXenes greatly affects their electronic characteristics and electrochemical properties [8–11]. For example, HF-MXenes have been reported to show excellent rate capability and high volumetric capacitance in acidic aqueous electrolytes [3], whereas low capacitance and poor rate capability were observed in non-aqueous solutions [12]. The nature and content of the MXene surface terminations are highly dependent on the synthetic route and post-synthesis treatment [13], and designing new synthesis routes for MXenes is an important challenge in terms of tuning their surface groups.

In 2019, a new method to prepare MXenes using a Lewis acid molten salt was reported [14], which attracted wide attention from researchers due to its great potential to tune the surface chemistry. By adjusting the Lewis acid melt composition, this molten salt synthesis route allows for the preparation of MXenes terminated with surface groups such as Cl, Br and I [15]. This method makes it feasible to produce new types of MXenes that are difficult or even impossible to prepare using conventional synthesis routes such as HF etching. Thus, the range of MAX phase precursors that can be used has been widened, offering interesting opportunities for tuning the surface chemistry and producing MS-MXenes that may function as a high-rate electrode in a non-aqueous system.

It is well known that the electrochemical performance of MXenes is highly dependent on the nature of the electrolyte [16,17]. In 2019, Wang et al. investigated the electrochemical properties of HF-$Ti_3C_2T_x$ as anodes for Li-ion batteries in three different electrolytes, and observed a doubling in capacity when moving from nitrile- and sulfoxide- to carbonate-based solvents [18]. In the present paper, Li-ion intercalation in Cl- and O-terminated MS-$Ti_3C_2T_x$ MXene used as negative electrode

* Corresponding authors.
E-mail addresses: pierre-louis.taberna@univ-tlse3.fr (P.-L. Taberna), patrice.simon@univ-tlse3.fr (P. Simon).

https://doi.org/10.1016/j.elecom.2023.107453
Received 28 November 2022; Received in revised form 2 February 2023; Accepted 5 February 2023
Available online 7 February 2023

was studied in nitrile-based electrolytes. The results show that using an acetonitrile-based electrolyte enables higher conductivity, while presenting low coulombic efficiency due to the electrolyte reduction occurring at low potential and the absence of solid electrolyte interphase (SEI) formation; however, the coulombic efficiency could be significantly improved by increasing the Li salt concentration. The results highlight the influence of the combination of surface terminations and electrolyte composition on the electrochemical performance of MXene materials, and pave the way for the design of electrodes for high-power performance applications.

2. Experimental

2.1. Preparation of MS-$Ti_3C_2T_x$

Ti_3AlC_2 (11 tech, CAS # 196506–01-1) was used as the MAX phase precursor, $CuCl_2$ (Sigma-Aldrich, CAS # 7447–39-4) was selected as the main etching molten salt while NaCl/KCl was used as the supporting electrolyte. The above chemicals were mixed in a Ti_3AlC_2:$CuCl_2$:NaCl:KCl = 1:3:2:2 M ratio, and then annealed inside an Ar-protected furnace at 680 °C for 24 h. After cooling to room temperature, the samples were washed with deionized water to remove the excess molten salt and then further immersed in a 0.1 M APS ($(NH_4)_2S_2O_8$, Sigma-Aldrich, CAS # 7727–54-0) solution for 4 h to dissolve the residual Cu. In the final step, the above product was washed with a large amount of deionized water to remove the residual APS, followed by drying under vacuum at 80 °C for 12 h.

2.2. Physical characterization

X-ray diffraction (XRD) data were collected by a D4 X-ray diffractometer (Bruker, Germany) equipped with CuKα radiation (λ = 0.154 nm). The morphology of the MXenes was observed using a scanning electron microscope (SEM) JSM 7100F (JEOL, Japan) with energy-dispersive X-ray spectroscopy (EDX) capabilities. Temperature-programmed desorption (TPD) was performed under an inert atmosphere (Ar, 100 ml min^{-1}). The sample (10–20 mg) was placed in a thermo-balance and heat-treated up to 1300 °C at a rate of 10 °C min^{-1}. The decomposition products (evolved gases) were monitored by online mass spectrometry (Skimmer, Netzsch, Germany).

2.3. Electrochemical measurements

APS-treated MS-$Ti_3C_2T_x$ powder was mixed with a binder and a conductive additive to prepare the working electrodes. 80 wt% of MXene powder was mixed with 15 wt% of carbon black and 5 wt% of PTFE binder and then calendared into films. The electrode films were dried in a vacuum oven at 80 °C for at least 10 h. A Cu disk was used as a current collector with an electrode mass loading of ~ 1.2 mg cm^{-2}. To prepare the counter electrode, YP-50 activated carbon (Kuraray, CAS #1333–86-4) was mixed with 5 % polytetrafluoroethylene binder, rolled into a free-standing film, and cut into disc-shaped electrodes. Two layers of porous borosilicate glass fibers 260 μm thick (Whatman GF/B) were used as the separator. A conventional three-electrode setup was assembled inside a glove box (O_2 < 0.1 ppm and H_2O < 0.1 ppm), with APS-treated MS-$Ti_3C_2T_x$ as the working electrode, YP50 active carbon as the counter electrode and silver wire as a quasi-reference electrode. All electrochemical characterizations were performed at room temperature using a multichannel VMP3 electrochemical workstation (Biologic, S. A.). Electrochemical impedance spectroscopy (EIS) measurements were carried out in a frequency range from 200 kHz down to 10 mHz, at an open circuit potential with an alternating voltage amplitude of 10 mV.

To evaluate the conductivity of the above electrolytes, a conductivity cell with separate double Pt sheet electrodes was purchased from Metrohm. The two Pt electrodes were fully immersed in the above electrolytes inside the glove box and then connected to the Biologic electrochemical workstation. Electrochemical impedance spectroscopy (EIS) measurements were performed at 1 kHz to obtain the resistance of the above electrolytes at room temperature (300 K). The cell conductivity was first calibrated to obtain the cell constant at 300 K using three standard saturated KCl solutions—their ionic conductivities were 10, 98 and 1413 μS cm^{-1}, respectively. Then the conductivity of the solution can be calculated using the following equation:

$$\sigma = 1/R^*_{1kHz}$$

where σ is the conductivity of the solution (S cm^{-1}), R_{1kHz} is the measured resistance of the solution (ohm) at 1 kHz, and K_{cell} is the cell constant (cm^{-1}), determined from the measurements carried out with the standard KCl solutions.

3. Results and discussion

3.1. Material characterization of $Ti_3C_2T_x$

Fig. 1(a) shows the XRD patterns of the pristine Ti_3AlC_2 MAX phase precursor before (black line) and after (green line) etching by $CuCl_2$, and after washing in APS to remove Cu (blue line). Compared to the pristine Ti_3AlC_2 precursor, most of the diffraction peaks disappeared immediately after $CuCl_2$ molten salt etching; combined with the shift of the intense (0 0 2) peak from 9.64° to 7.96°, this suggests the successful etching of the Al layer from Ti_3AlC_2 to form layered Ti_3C_2 with the interlayer distance expanded from 9.20 (MAX) to 11.08 Å (MXene). The sharp peaks located at 43.29°, 50.43° and 74.13° can be indexed to Cu metal, and these disappeared directly after further APS washing as a result of the successful removal of Cu. The SEM image (see Fig. 1b) clearly shows a visible lamellar structure a few layers thick with an accordion-like morphology, which is the traditional morphology of MXene [15]. Energy-dispersive spectroscopy (EDS) measurements of MS-$Ti_3C_2T_x$ (Fig. 1c and 1d) show the presence of small residual weak Al and Cu peaks corresponding to<1 at.%, which is consistent with the previous XRD results. EDS semi-quantitative analysis confirms the presence of Cl (16.8 at.%) and O (20.5 at.%), which are highly likely to be present as surface groups. In addition, the elemental mapping of Ti, Cl and O (Fig. 1d) shows a uniform distribution, suggesting that some of the original halogen-terminated groups have been replaced by oxygen-containing functionality during the APS washing.

To identify the different termination species, temperature-programmed desorption, coupled with mass spectroscopy measurements (TPD-MS), was performed on APS-treated MS-$Ti_3C_2T_x$. In the 25–900 °C temperature range, the weight loss associated with the gas evolution of CO_2, CO and H_2O shows that O-containing and Cl groups as well as adsorbed/intercalated water are the main components of the MS-$Ti_3C_2T_x$ MXene surface (see Fig. 1e). The H_2O release observed below 400 °C, for all samples, corresponds to surface-adsorbed and intercalated water derived from the washing step [15]. The important CO_2 gas release at 100–600 °C is assumed to originate from the oxidation of the carbon in Ti_3C_2 by the APS, which further confirms the large amount of oxygen-containing functional groups. The significant release of CO at ~ 800 °C demonstrates the degradation of the MXene material, where the structure is converted into the cubic TiC_y [19] form, while some C reacts with the remaining O-functional groups [20]. Quantitative analysis of CO_2, H_2O and CO derived from TPD-MS measurements shows a total oxygen content of 15.8 % (Table S1).

3.2. Electrochemical characterization

3.2.1. Electrochemical characterization of LiTFSI in CH_3CN electrolyte

Fig. 2(a) compares the conductivity of different types of electrolytes involving LiFSI (lithium bis(fluorosulfonyl)imide) and LiTFSI (lithium bis(trifluoromethanesulfonyl)imide) salts in nitrile- and carbonate-based solvents. As expected, LiTFSI and LiFSI in ACN electrolytes

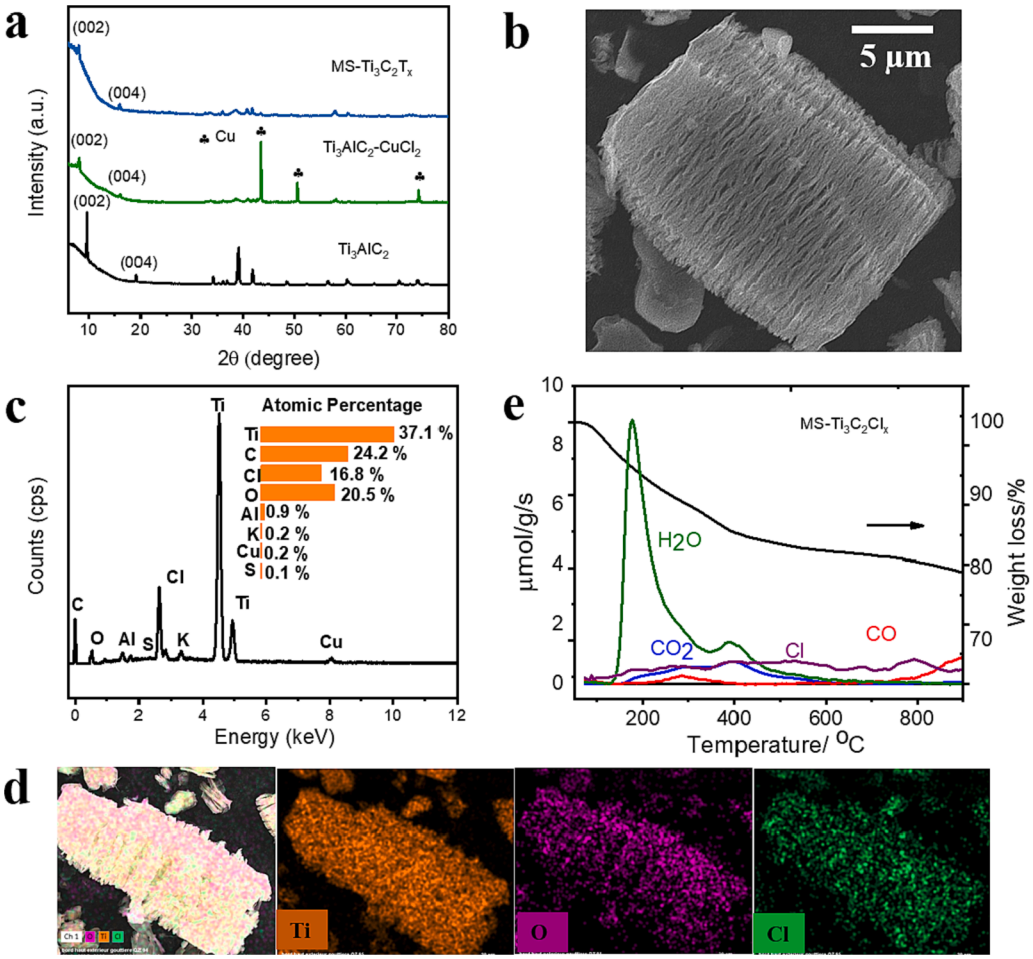

Fig. 1. Characterization of MS-$Ti_3C_2T_x$: (a) XRD patterns of pristine Ti_3AlC_2 before (black line) and after reaction with $CuCl_2$ (green line) followed by washing in 0.1 M $(NH_4)_2S_2O_8$ solution (blue line); (b) SEM image; (c) EDS analysis; (d) SEM images and corresponding EDS mapping; and (e) TPD-MS measurements of MS-$Ti_3C_2T_x$ at temperatures up to 900 °C.

achieve a higher conductivity than the other types of electrolytes with the same concentration but in different solvents (1 M LP30: 1 M $LiPF_6$ in ethylene carbonate/dimethyl carbonate with 1:1 vol ratio and 1 M LiTFSI in propylene carbonate (PC)). However, the conductivity of LiTFSI in ACN decreases continuously from 37.1 to 2.1 mS cm^{-1} as the concentration increases from 1 M to 4 M, which is similar to the results for LiFSI in ACN (where the conductivity decreases from 42.2 to 14.6 mS cm^{-1} as the concentration increases from 1 M to 4 M). The maximum potential window of LiTFSI in acetonitrile (ACN) electrolyte was evaluated using a three-electrode cell configuration with a small Pt foil as the working electrode, a Pt foil with a large surface area as the counter electrode and an Ag wire as a quasi-reference electrode (Fig. S1), and tested under an Ar atmosphere. As shown in Fig. 2(b), for both 1 M and 4 M LiTFSI in ACN electrolytes, the high current density measured above 3.0 V vs Ag and below −3.2 V vs Ag results in a working potential window of about 6.2 V. However, both the reduction and oxidation currents are smaller in 4 M LiTFSI in ACN than in 1 M LiTFSI in ACN electrolyte, indicating improved electrolyte stability as the electrolyte concentration increases. After 5 cycles at 20 mV s^{-1}, as shown in Fig. 2 (c), the 1 M LiTFSI in ACN electrolyte turned yellow, while the two platinum disk electrodes became black. By contrast, the 4 M LiTFSI in ACN electrolyte (see Fig. 2d), remained transparent after testing and the platinum electrodes were still bright. Those visual inspections are very much in line with better electrochemical stability for a higher concentration of LiTFSI, as no visible by-products are formed in the electrolyte or on the platinum electrodes. Yamada et al. reported that improved electrochemical stability in such superconcentrated solutions arises from a peculiar organized electrolyte structure with metal cations coordinated by the anions and solvent molecules, forming aggregates and contact ion pairs, while only a few free ACN molecules are present [21].

Fig. 3 shows CVs of MS-$Ti_3C_2T_x$ electrodes tested using LiTFSI in ACN electrolytes with different concentrations of LiTFSI ranging from 1 M to 4 M. At high scan rates such as 500 mV s^{-1} the CV area becomes smaller as the electrolyte concentration increases, which can be explained by the decrease in ionic conductivity as shown in Fig. 2(a). Nevertheless, with the 1 M LiTFSI-ACN electrolyte, a low coulombic efficiency of 39 % is obtained at a low scan rate of 1 mV s^{-1} due to its lower cathodic stability compared to 4 M LiTFSI-ACN. On increasing the electrolyte concentration from 1 M to 4 M, the coulombic efficiency can be improved from 39 % to 88 %, at 1 mV s^{-1} (Fig. S2). This may be attributed to the lower ionic conductivity; alternatively, the smaller number of free ACN molecules on increasing the concentration of LiTSFI could also play a role here [21,22]. Interestingly, MS-$Ti_3C_2T_x$ in 2 M LiTFSI electrolyte achieves the highest capacity of 136 mAh g^{-1} (272F g^{-1}) compared to other concentrations (see Table S2), while maintaining a high power performance of 87 mAh g^{-1} (174F g^{-1}) with 63 % of capacity retention. The latter figure was only 27 % and 11 % in LP30 and 1 M LiTFSI-PC electrolytes, respectively. Despite the slightly decreased ionic conductivity of 2 M LiTFSI in ACN compared to the 1 M electrolyte, the increased Li-ion concentration allows more Li^+ to be intercalated inside the MXene layers or absorbed to the MXene surface. However, with a further increase in Li ion concentration, the ionic conductivity is decreased, resulting in lower kinetic behavior and lower capacity.

Figure S3 compares the Cvs of MS-$Ti_3C_2T_x$ in 2 M LiTFSI-ACN

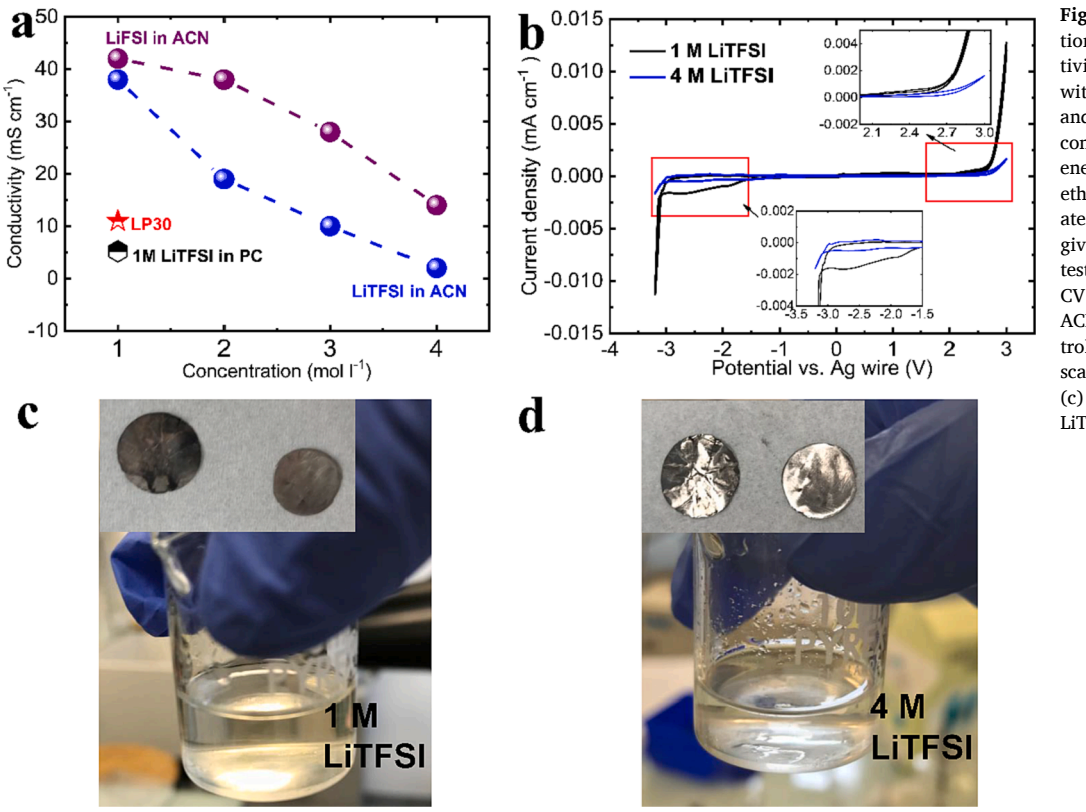

Fig. 2. Electrochemical characterization of electrolytes. (a) Ionic conductivity of different types of electrolytes with different concentrations of LiTFSI and LiFSI salts in acetonitrile. The conductivity of 1 M LiTFSI in propylene carbonate and LP30 (1 M $LiPF_6$ in ethylene carbonate/dimethyl carbonate with 1:1 vol ratio) electrolyte are given for reference. Blank electrolyte test of LiTFSI in ACN electrolyte: (b) CV profiles of 1 M and 4 M LiTFSI in ACN scanned at 5 mV s^{-1}; Blank electrolytes and platinum electrodes after scanning at 20 mV s^{-1} for 5 cycles for (c) 1 M LiTFSI in ACN and (d) 4 M LiTFSI in ACN.

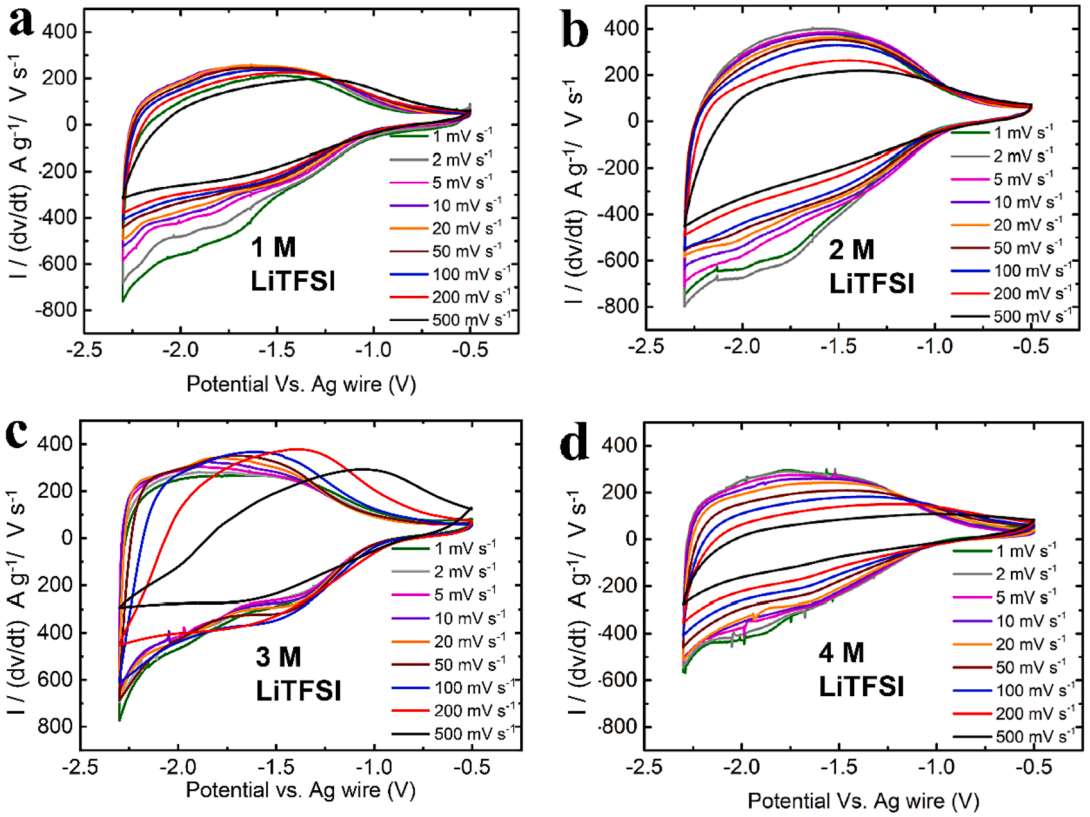

Fig. 3. CV curves of MS-$Ti_3C_2T_x$ recorded at various potential scan rates from 1 to 500 mV s^{-1} within a potential window from −2.3 V to −0.5 V vs Ag for LiTFSI in ACN electrolytes at different concentrations: (a) 1 M, (b) 2 M, (c) 3 M and (d) 4 M.

electrolytes recorded at several potential scan rates with different negative potential cut-offs. As shown in Fig. S3a, the electrolyte decomposition starts at a low scan rate below −2.5 V vs the reference (Ag wire). Thereafter, the negative potential window is limited to −2.3 V vs the reference (Fig. 3b), the electrochemical signature is well preserved and the capacity contribution is mainly effective in the −2.3 V to −1.0 V vs Ag potential range. However, the capacity is greatly reduced (65 % loss) when the cathodic potential cut-off is limited to −2 V vs Ag (Fig. S3b), indicating that the main capacity contribution comes from the low potential range region, lower than −2 V.

MS-$Ti_3C_2T_x$ has also been tested in LP30 and 1 M LiTFSI-PC electrolytes as shown in Fig. S4, using the same cell set-up. Although MS-$Ti_3C_2T_x$ in both electrolytes has a similar electrochemical signature, MS-$Ti_3C_2T_x$ shows a poor rate capability in these two electrolytes compared to LiTFSI in ACN. This expected result is explained by the lower ionic conductivity of PC-based electrolytes vs ACN-based ones (see Fig. 2a, 2 M LiTFSI-ACN: 22.1 mS cm^{-1}, LP30: 11.0 mS cm^{-1} and 1 M LiTFSI-PC: 5.2 mS cm^{-1}).

3.2.2. *Electrochemical characterization of LiFSI in CH_3CN electrolyte*

MS-$Ti_3C_2T_x$ was also tested using 1 M LiFSI in ACN electrolyte due to its high conductivity of 43 mS cm^{-1} (see Fig. 2a). Fig. 4(a) shows the cyclic voltammetry profiles of MS-$Ti_3C_2T_x$ collected at potential scan rates from 2 to 500 mV s^{-1}. Remarkably, the CV signature of MS-$Ti_3C_2T_x$ remains capacitive even at a high scan rate of 500 mV s^{-1}, giving 110 mAh g^{-1} (220F g^{-1}) at 2 mV s^{-1} and 95 mAh g^{-1} (190F g^{-1}) at 500 mV s^{-1}, with a high capacity retention of 88 %. Galvanostatic charge/discharge measurements (Fig. 4b) confirm the unique electrochemical signature of the electrode in 1 M LiFSI-ACN non-aqueous electrolyte, with a sloping voltage profile within the potential range −0.5 to −2.3 V versus Ag wire, as expected from the cyclic voltammetry profiles. However, as shown in Fig. S5, the increase in lithium-salt concentrations to 2 M and 3 M LiFSI in ACN results in a similar capacity of 99 and 101 mAh g^{-1} at 2 mV s^{-1} with lower capacity retention of 65 % and 61 %, respectively. Fig. 4(c) compares the change in the MS-$Ti_3C_2T_x$ capacitance and capacity with scan rates calculated from cyclic voltammetry at various potential scan rates in 1 M LiFSI in ACN, 2 M LiTFSI in ACN and LP30 electrolytes. The capacitance of MS-$Ti_3C_2T_x$ for 2 M LiTFSI in ACN electrolyte reaches 123 mAh g^{-1} (245F g^{-1}) at a low scan rate of 5 mV s^{-1}, combined with a coulombic efficiency of 76 % (see Fig. S2). The capacitance remains at 87 mAh g^{-1} (174F g^{-1}) and the coulombic efficiency goes up to 100 % at a high scan rate of 500 mV s^{-1}, corresponding to a capacitance retention of 71 % as compared to the value of 5 mV s^{-1}, which is much higher than the capacitance retention of 21 % measured in LP30. In contrast, despite a slightly lower maximum capacity of 110 mAh g^{-1} (220F.g^{-1}) and lower coulombic efficiency (76 %), MS-$Ti_3C_2T_x$ with 1 M LiTFSI in ACN electrolyte achieves the best power capability with 95 mAh g^{-1} (192F g^{-1}) at 500 mV s^{-1} (equivalent to 900C) with a capacitance retention of 88 %. It also outperforms the electrochemical performance of HF-$Ti_3C_2T_x$ (prepared by the conventional LiF/HCl etching method) in LiTFSI-PC electrolyte under similar conditions (see Fig. S6) [18], which represents the best power performance for a MXene electrode reported so far in a non-aqueous electrolyte (see Table S3).

Fig. 4(d) shows the Nyquist plots of the MS-$Ti_3C_2T_x$ electrode recorded at various bias potentials in 1 M LiFSI-ACN electrolyte. It shows typical capacitive behavior with a small loop in the high-frequency region associated with low charge-transfer resistance (<5 O, Fig. 4d inset), followed by a rapid increase of the imaginary part at low frequencies, which is consistent with a pseudo-capacitive charge-storage mechanism for the MS-$Ti_3C_2T_x$ electrode. This further explains the high-power performance of the MS-$Ti_3C_2T_x$ MXene electrode with 1 M LiTFSI in ACN electrolyte.

4. Conclusion

In this study, the electrochemical behavior of Cl- and O-terminated

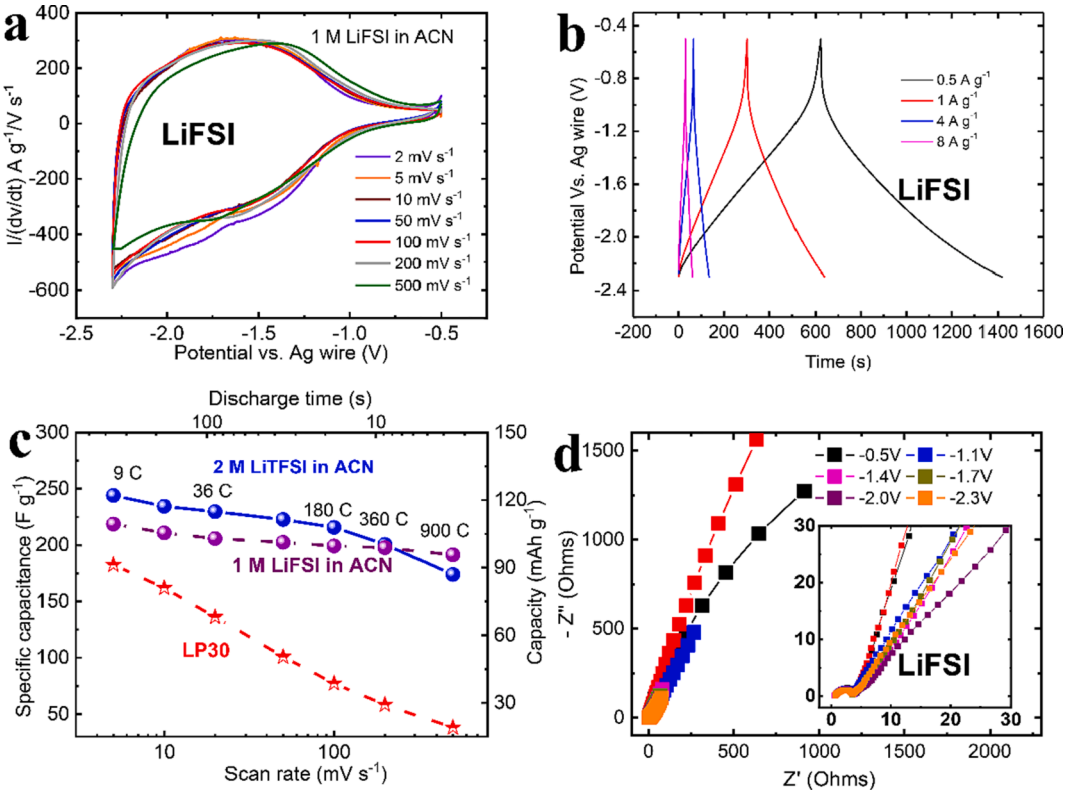

Fig. 4. Electrochemical characterization of MS-$Ti_3C_2T_x$ using 1 M LiFSI in ACN electrolyte. (a) CV curves of MS-$Ti_3C_2T_x$ recorded at various potential scan rates from 2 to 500 mV s^{-1}. (b) Galvanostatic charge/discharge curves at current densities from 0.5 to 8 A g^{-1}. (c) Specific capacitance and capacity evolution with scan rates for different electrolytes. (d) Electrochemical impedance spectroscopy plots recorded at various bias potentials.

MS-$Ti_3C_2T_x$ was evaluated in different electrolytes prepared from Li salts (LiFSI, LiTFSI) dissolved in nitrile-based solvents. MS-$Ti_3C_2T_x$ shows high power performance with the LiTFSI in ACN electrolyte, but low coulombic efficiency. On increasing the electrolyte concentration from 1 M to 4 M LiTFSI, the coulombic efficiency was drastically improved from 39 % to 88 %, thanks to the enhanced electrochemical stability of the electrolyte. In contrast, MS-$Ti_3C_2T_x$ materials showed great power ability (87 mAh g^{-1} at 900C) when using 2 M LiTFSI in ACN electrolyte, combined with a decent coulombic efficiency. Moreover, when using 1 M LiFSI in ACN electrolyte with higher conductivity, the power performance could be further improved to 95 mAh g^{-1} at 900C, corresponding to a capacity retention of 88 % vs low-rate discharge. This study shows that properly matching the electrolyte composition to the electrode material offers new opportunities in the design of the next generation of high-rate materials for energy storage applications.

Declaration of Competing Interest

The authors declare that they have no known competing financial interests or personal relationships that could have appeared to influence the work reported in this paper. [Patrice Simon reports financial support was provided by European Research Council].

Data availability

Data will be made available on request.

Acknowledgements

L.L. was supported by European Research Council (ERC) Synergy Grant MoMa-Stor#951513. P.S. and P.L.T. acknowledge the support from Agence Nationale de la Recherche (Labex Store-ex) and ERC Synergy Grant MoMa-Stor #951513.

Appendix A. Supplementary material

Supplementary data to this article can be found online at https://doi.org/10.1016/j.elecom.2023.107453.

References

[1] B. Anasori, M.R. Lukatskaya, Y. Gogotsi, 2D metal carbides and nitrides (MXenes) for energy storage, Nat. Rev. Mater. 2 (2017) 1–17.
[2] M. Ghidiu, M.R. Lukatskaya, M.-Q. Zhao, Y. Gogotsi, M.W. Barsoum, Conductive two-dimensional titanium carbide 'clay'with high volumetric capacitance, Nature 516 (2014) 78–81.
[3] M.R. Lukatskaya, S. Kota, Z. Lin, M.-Q. Zhao, N. Shpigel, M.D. Levi, J. Halim, P.-L. Taberna, M.W. Barsoum, P. Simon, Ultra-high-rate pseudocapacitive energy storage in two-dimensional transition metal carbides, Nature, Energy 2 (2017) 1–6.
[4] L. Liu, P.-L. Taberna, B. Dunn, P. Simon, Future directions for electrochemical capacitors, ACS Energy Lett. 6 (2021) 4311–4316.
[5] M.R. Lukatskaya, O. Mashtalir, C.E. Ren, Y. Dall'Agnese, P. Rozier, P.L. Taberna, M. Naguib, P. Simon, M.W. Barsoum, Y. Gogotsi, Cation intercalation and high volumetric capacitance of two-dimensional titanium carbide, Science 341 2013 1502-1505.
[6] M. Naguib, M. Kurtoglu, V. Presser, J. Lu, J. Niu, M. Heon, L. Hultman, Y. Gogotsi, M.W. Barsoum, Two-dimensional nanocrystals produced by exfoliation of Ti3AlC2, Adv. Mater. 23 (2011) 4248–4253.
[7] L. Liu, M. Orbay, S. Luo, S. Duluard, H. Shao, J. Harmel, P. Rozier, P.-L. Taberna, P. Simon, Exfoliation and delamination of Ti3C2Tx MXene prepared via molten salt etching route, ACS Nano 16 (2022) 111–118.
[8] Q. Tang, Z. Zhou, P. Shen, Are MXenes promising anode materials for Li ion batteries? Computational studies on electronic properties and Li storage capability of Ti3C2 and Ti3C2X2 (X= F, OH) monolayer, J. Am. Chem. Soc. 134 (2012) 16909–16916.
[9] Y. Xie, M. Naguib, V.N. Mochalin, M.W. Barsoum, Y. Gogotsi, X. Yu, K.-W. Nam, X.-Q. Yang, A.I. Kolesnikov, P.R. Kent, Role of surface structure on Li-ion energy storage capacity of two-dimensional transition-metal carbides, J. Am. Chem. Soc. 136 (2014) 6385–6394.
[10] G.R. Berdiyorov, K.A. Mahmoud, Effect of surface termination on ion intercalation selectivity of bilayer Ti3C2T2 (T= F, O and OH) MXene, Appl. Surf. Sci. 416 (2017) 725–730.
[11] D. Li, X. Chen, P. Xiang, H. Du, B. Xiao, Chalcogenated-Ti3C2X2 MXene (X=O, S, Se and Te) as a high-performance anode material for Li-ion batteries, Appl. Surf. Sci. 501 (2020), 144221.
[12] R. Cheng, T. Hu, H. Zhang, C. Wang, M. Hu, J. Yang, C. Cui, T. Guang, C. Li, C. Shi, Understanding the lithium storage mechanism of Ti3C2T x MXene, J. Phys. Chem. C 123 (2018) 1099–1109.
[13] M. Naguib, M.W. Barsoum, Y. Gogotsi, Ten years of progress in the synthesis and development of MXenes, Adv. Mater. 33 (2021) 2103393.
[14] M. Li, J. Lu, K. Luo, Y. Li, K. Chang, K. Chen, J. Zhou, J. Rosen, L. Hultman, P. Eklund, Element replacement approach by reaction with Lewis acidic molten salts to synthesize nanolaminated MAX phases and MXenes, J. Am. Chem. Soc. 141 (2019) 4730–4737.
[15] Y. Li, H. Shao, Z. Lin, J. Lu, L. Liu, B. Duployer, P.O. Persson, P. Eklund, L. Hultman, M. Li, A general Lewis acidic etching route for preparing MXenes with enhanced electrochemical performance in non-aqueous electrolyte, Nat. Mater. 19 (2020) 894–899.
[16] C. Zhong, Y. Deng, W. Hu, J. Qiao, L. Zhang, J. Zhang, A review of electrolyte materials and compositions for electrochemical supercapacitors, Chem. Soc. Rev. 44 (2015) 7484–7539.
[17] L. Liu, Z. Lin, J.-Y. Chane-Ching, H. Shao, P.-L. Taberna, P. Simon, 3D rGO aerogel with superior electrochemical performance for K–ion battery, Energy Storage Mater. 19 (2019) 306–313.
[18] X. Wang, T.S. Mathis, K. Li, Z. Lin, L. Vlcek, T. Torita, N.C. Osti, C. Hatter, P. Urbankowski, A. Sarycheva, Influences from solvents on charge storage in titanium carbide MXenes, Nature, Energy 4 (2019) 241–248.
[19] B.C. Wyatt, S.K. Nemani, K. Desai, H. Kaur, B. Zhang, B. Anasori, High-temperature stability and phase transformations of titanium carbide (Ti3C2T x) MXene, J. Phys. Condens. Matter 33 (2021), 224002.
[20] M. Seredych, C.E. Shuck, D. Pinto, M. Alhabeb, E. Precetti, G. Deysher, B. Anasori, N. Kurra, Y. Gogotsi, High-temperature behavior and surface chemistry of carbide MXenes studied by thermal analysis, Chem. Mater. 31 (2019) 3324–3332.
[21] Y. Yamada, K. Furukawa, K. Sodeyama, K. Kikuchi, M. Yaegashi, Y. Tateyama, A. Yamada, Unusual stability of acetonitrile-based superconcentrated electrolytes for fast-charging lithium-ion batteries, J. Am. Chem. Soc. 136 (2014) 5039–5046.
[22] Y. Yamada, J. Wang, S. Ko, E. Watanabe, A. Yamada, Advances and issues in developing salt-concentrated battery electrolytes, Nature, Energy 4 (2019) 269–280.